






# Flavour-Dependent Chemical Freeze-Out of Light Nuclei in Relativistic Heavy-Ion Collisions

Rishabh Sharma <sup>a</sup>, Fernando Antonio Flor <sup>b</sup>, Sibaram Behera <sup>a</sup>, Chitrasen Jena <sup>a</sup>, Helen Caines <sup>b</sup>

<sup>a</sup>Department of Physics, Indian Institute of Science Education and Research (IISER) Tirupati, Tirupati, 517619, Andhra Pradesh, India

<sup>b</sup>Wright Laboratory, Yale University, New Haven, CT, 06520, USA

## Abstract

We study the production of light nuclei in Au+Au collisions at  $\sqrt{s_{NN}} = 7.7 - 200$  GeV and Pb+Pb collisions at  $\sqrt{s_{NN}} = 2.76$  and 5.02 TeV within a flavour-dependent freeze-out framework, assuming different flavoured hadrons undergo separate chemical freeze-out. Using the Thermal-FIST package, thermal parameters extracted from fits to various sets of hadron yields, including and excluding light nuclei, are used to calculate the ratios of the yields of light nuclei, namely,  $d/p$ ,  $\bar{d}/\bar{p}$ ,  $t/p$ , and  $t/d$ . A comparison with data from the STAR and ALICE collaborations shows that a sequential freeze-out scenario provides a better description of light nuclei yield ratios than the traditional single freeze-out approach. These results suggest the flavour-dependent chemical freeze-out for final state light-nuclei production persists in heavy-ion collisions at both RHIC and LHC energies.

**Keywords:** Light Nuclei, Sequential Flavour Freeze-out, Statistical Hadronization

## 1. Introduction



In relativistic heavy-ion collisions, nuclear matter is heated to extreme temperatures and energy densities, forming a deconfined state of quarks and gluons known as the quark-gluon plasma (QGP) [1–4]. The high energy density created in the collisions results in a strong pressure gradient, causing a rapid expansion and cooling of the produced QGP. As the system evolves, it transitions to an interacting gas of hadrons. This hadronic fireball continues to expand and eventually undergoes chemical freeze-out, where inelastic collisions cease, fixing the relative abundances of hadrons. Elastic collisions after chemical freeze-out keep the system in thermal equilibrium until the kinetic freeze-out [5].

The Hadron Resonance Gas (HRG) model has been widely used to study hadron production in heavy-ion collisions [6–8]. In its simplest formulation, with just a few thermal parameters — volume ( $V$ ), chemical freeze-out temperature ( $T_{\text{ch}}$ ), and chemical potentials ( $\mu_B$ ,  $\mu_Q$ , and  $\mu_S$  corresponding to the conserved QCD charges, baryon number  $B$ , electric charge  $Q$ ,

and strangeness  $S$ , respectively) — it has been remarkably successful in describing the abundances of various hadrons produced across wide range of collision systems and energies. A comparison of transverse momentum ( $p_T$ )-integrated hadron yields ( $dN/dy$ ) with the predictions from the HRG allows the estimation of these parameters and defines the thermodynamic state of the system at chemical freeze-out.

Traditionally, chemical freeze-out is understood as the process where all the hadrons in the fireball freeze-out at the same temperature (1CFO). However, this process can be more complex where particles may freeze out at different times, leading to a sequential freeze-out. Hadrochemical analyses [9–11] and high-precision continuum-extrapolated lattice QCD calculations [12, 13] have suggested that flavour-dependent chemical freeze-out temperatures emerge in the QCD phase transition crossover region. This implies that quark flavours, such as light and strange quarks, may freeze out at different temperatures, establishing a flavour hierarchy during the transition. Scenarios where strange-flavour hadrons freeze out earlier than light-flavour hadrons (2CFO) have been studied and found to describe the data better compared to a 1CFO scenario [9, 14, 15]. It has been reported that  $T_{\text{ch}}$  for light hadrons is approximately  $150.2 \pm 2.6$  MeV, while for strange hadrons it is around  $165.1 \pm 2.7$  MeV, at vanishing  $\mu_B$  [14].

*Email addresses:*

rishabhsharma@students.iisertirupati.ac.in (Rishabh Sharma ) , fernando.flor@yale.edu (Fernando Antonio Flor )

Preprint submitted to Elsevier

January 2, 2025

Although the HRG model has shown good agreement with the  $dN/dy$  of light nuclei at the LHC energies, the underlying production mechanism remains unclear [16, 17]. Light nuclei have very low binding energies, and it remains puzzling how such fragile objects could exist in the hadronic fireballs, where, at the time of chemical freeze-out, the temperatures are well above their binding energies [18]. However, it has been argued that the relative yield of nuclei is determined by the entropy per baryon, which is fixed at chemical freeze-out [16, 19, 20]. Therefore, entropy conservation governs the production yields of light nuclei. Recently, at RHIC energies, the STAR collaboration reported that although the thermal model describes the  $d/p$  yield ratio, it systematically overestimates the  $t/p$  ratio [21, 22].

A recent study of light nuclei production at RHIC energies indicated a distinct freeze-out of light nuclei, reporting freeze-out temperatures of  $150.2 \pm 6$  MeV for light hadrons,  $165.1 \pm 2.7$  MeV for strange hadrons, and  $141.7 \pm 1.4$  MeV for light nuclei [17]. Given the similarity between the freeze-out temperature of light nuclei and that of light hadrons, it is reasonable to assert that light nuclei form near the chemical freeze-out of light hadrons in the 2CFO scenario, as shown in [11].

In this letter, we study the impact of the 2CFO scenario on the production of light nuclei. Chemical freeze-out parameters were estimated by performing thermal fits to the  $dN/dy$  of various hadrons in the most central Au+Au collisions at  $\sqrt{s_{\text{NN}}} = 7.7 - 200$  GeV and Pb+Pb collisions at  $\sqrt{s_{\text{NN}}} = 2.76$  and 5.02 TeV. In addition, we explore how the chemical freeze-out is affected by the inclusion of  $dN/dy$  of light nuclei,  $d(\bar{d})$ ,  $t$ ,  ${}^3\text{He}({}^3\bar{\text{He}})$ , in the thermal fits. These parameters are used to compare the calculations of 1CFO and 2CFO scenarios with the experimental data of light nuclei yield ratios from the STAR and ALICE collaborations. The letter is organized as follows: Sec. 2 describes the HRG model, Sec. 3 discusses our findings with respect to light nuclei production, and we present a summary of our results in Sec. 4.

## 2. Hadron Resonance Gas Model

The analysis in this letter was performed using the open-source Thermal-FIST (Thermal, Fast and Interactive Statistical Toolkit) package, a versatile framework designed for studying particle production in high-energy collisions within the HRG model [23]. The Thermal-FIST offers a range of capabilities, including the computation of hadron yields, ratios, and fluctuations and the ability to perform thermal fits using the

Canonical Ensemble (CE) and the Grand Canonical Ensemble (GCE). In our analysis, we used the GCE framework, where the QCD conserved charges,  $B$ ,  $Q$ , and  $S$  are not conserved strictly but are maintained on average through their corresponding chemical potentials,  $\mu_B$ ,  $\mu_Q$ , and  $\mu_S$ , respectively. Particle yields in GCE are described by the equation:

$$N_i = \frac{g_i V}{2\pi^2} \int_0^\infty \frac{p^2 dp}{\exp\left(\frac{E_i - \mu_i}{T_{\text{ch}}}\right) \pm 1}, \quad (1)$$

where  $g_i$  is the degeneracy factor,  $p$  is the particle momentum,  $E_i = \sqrt{p^2 + m_i^2}$  is the energy, and  $\mu_i = B\mu_B + Q\mu_Q + S\mu_S$  is the chemical potential. The + and - signs correspond to fermions and bosons, respectively.

We used the PDG2020 [24] hadronic spectrum available in Thermal-FIST v1.4.2. The  $dN/dy$  of identified hadrons ( $\pi^\pm$ ,  $K^\pm$ ,  $K_s^0$ ,  $p(\bar{p})$ ,  $\phi$ ,  $\Lambda(\bar{\Lambda})$ ,  $\Xi^-(\bar{\Xi}^+)$ , and  $\Omega^-(\bar{\Omega}^+)$ ) and light nuclei ( $d(\bar{d})$ , and  $t$  or  ${}^3\text{He}({}^3\bar{\text{He}})$ ) in 0–10% central Au+Au collisions at  $\sqrt{s_{\text{NN}}} = 7.7, 11.5, 19.6, 27, 39,$  and 200 GeV and Pb+Pb collisions at  $\sqrt{s_{\text{NN}}} = 2.76$  and 5.02 TeV were used in the thermal fits from the STAR and ALICE collaborations [21, 22, 25–34]. For Au+Au collisions at  $\sqrt{s_{\text{NN}}} = 200$  GeV, the 0–5% values were used for  $K_s^0$ ,  $\Lambda(\bar{\Lambda})$ ,  $\Xi^-(\bar{\Xi}^+)$ , and  $\Omega^-(\bar{\Omega}^+)$  yields due to the binning of the experimental data. For brevity, we adopt a shorthand notation where the symbol of a particle (e.g.  $p$ ) represents both the particle ( $p$ ) and its corresponding anti-particle ( $\bar{p}$ ). This convention is followed throughout this letter unless explicitly stated otherwise.

The free parameters in our thermal fits are  $T_{\text{ch}}$ ,  $\mu_B$ , and  $V$ . The chemical potentials  $\mu_Q$  and  $\mu_S$  were constrained using the conditions, net  $Q/B = 0.4$  and net  $S = 0$ , ensuring conservation of electric charge and strangeness. We set the strangeness fugacity factor,  $\gamma_s = 1$ , assuming complete strangeness equilibrium. Further, we applied quantum statistics to all particles, and the finite widths of resonances were incorporated by considering an energy-dependent Breit-Wigner (eBW) distribution in our fitting procedure [35]. The particle sets considered in the analysis are as follows:

- 1CFO scenario:
  - $\pi$ ,  $K$ ,  $K_s^0$ ,  $p$ ,  $\phi$ ,  $\Lambda$ ,  $\Xi$ , and  $\Omega$  [*hadrons*]
  - $\pi$ ,  $K$ ,  $K_s^0$ ,  $p$ ,  $\phi$ ,  $\Lambda$ ,  $\Xi$ ,  $\Omega$ ,  $d$ , and  $t$  or  ${}^3\text{He}$  [*hadrons+nuclei*]
- 2CFO scenario:
  - $\pi$ ,  $K$ , and  $p$  [*light hadrons*]

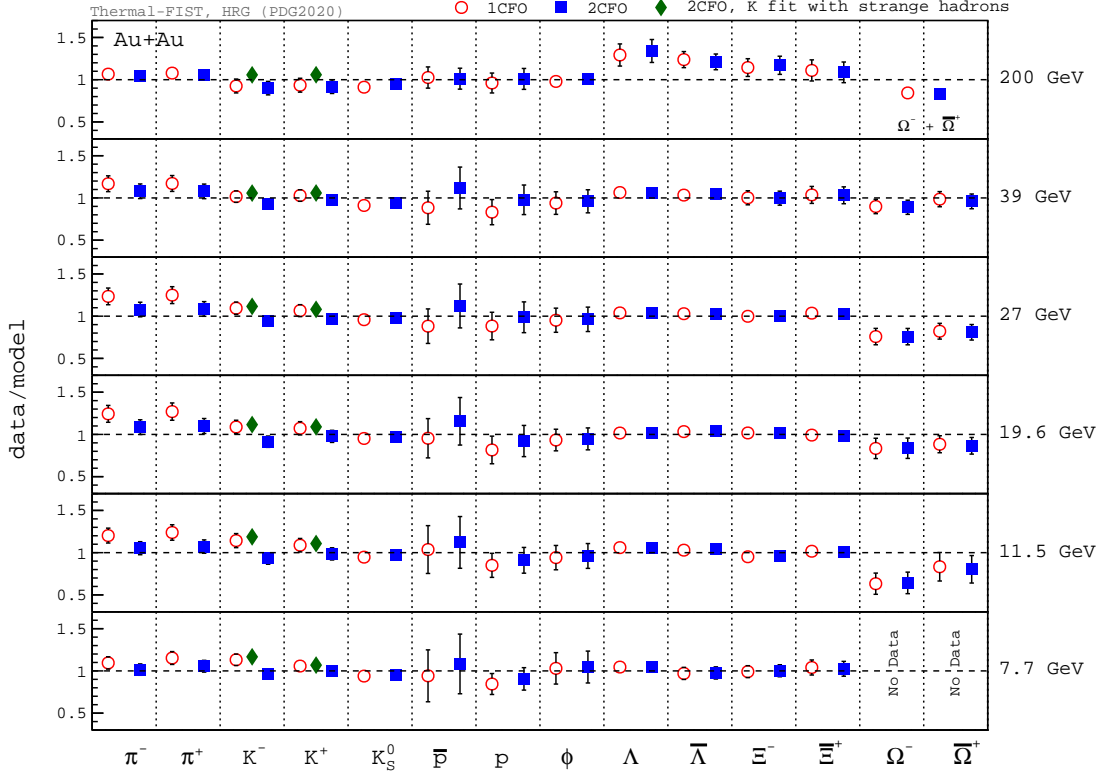


Figure 1: Ratios of experimental data to thermal model fit to  $\pi$ ,  $K$ ,  $K_s^0$ ,  $p$ ,  $\phi$ ,  $\Lambda$ ,  $\Xi$ , and  $\Omega$  in 0–10% centrality of Au+Au collisions at  $\sqrt{s_{NN}} = 7.7 - 200$  GeV ( $K_s^0$ ,  $\Lambda$ ,  $\Xi$ , and  $\Omega$  yields at  $\sqrt{s_{NN}} = 200$  GeV were measured in 0–5% centrality). The 1CFO yield calculations are shown as open red circles while the 2CFO calculations are shown as solid blue squares. The solid green diamonds indicate the case where the charged kaons were included in the *strange hadrons* set.

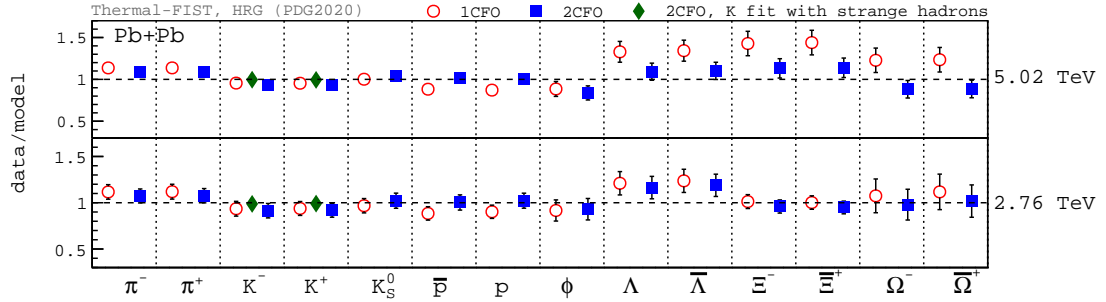


Figure 2: Ratios of experimental data to thermal model fit to  $\pi$ ,  $K$ ,  $K_s^0$ ,  $p$ ,  $\phi$ ,  $\Lambda$ ,  $\Xi$ , and  $\Omega$  in 0–10% centrality of Pb+Pb collisions at  $\sqrt{s_{NN}} = 2.76$  and 5.02 TeV following the same symbol convention as Fig. 1.

- $\pi$ ,  $p$ ,  $d$ , and  $t$  or  $^3\text{He}$  [*light hadrons+nuclei*]
- $K$ ,  $K_s^0$ ,  $\phi$ ,  $\Lambda$ ,  $\Xi$ , and  $\Omega$  [*strange hadrons*]

Including  $K$  in the *light hadrons* fit prevents too few statistical degrees of freedom, as it has been shown that it does not significantly impact  $T_{\text{ch}}$  [36, 14]. Further-

more, to study the effect of light nuclei on the chemical freeze-out, we performed thermal fits to various particle species, incorporating light nuclei as detailed above.

The freeze-out parameters obtained from the thermal fits to the *hadrons(+nuclei)* and *light hadrons(+nuclei)* particle sets were used to calculate the nuclei yield ra-

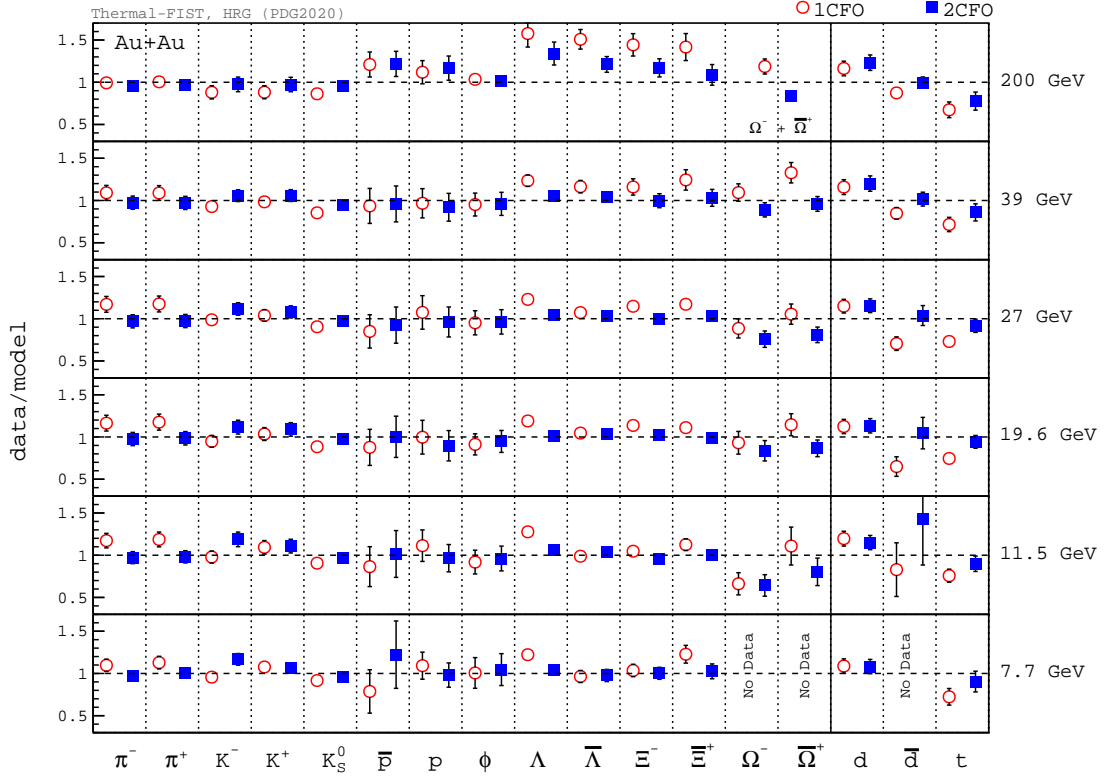


Figure 3: Ratios of experimental data to thermal model fit to  $\pi$ ,  $K$ ,  $K_s^0$ ,  $p$ ,  $\phi$ ,  $\Lambda$ ,  $\Xi$ ,  $\Omega$ ,  $d$ , and  $t$  in 0–10% centrality of Au+Au collisions at  $\sqrt{s_{NN}} = 7.7 - 200$  GeV ( $K_s^0$ ,  $\Lambda$ ,  $\Xi$ , and  $\Omega$  yields at  $\sqrt{s_{NN}} = 200$  GeV were measured in 0–5% centrality). The 1CFO yield calculations are shown as open red circles while the 2CFO calculations are shown as solid blue squares.

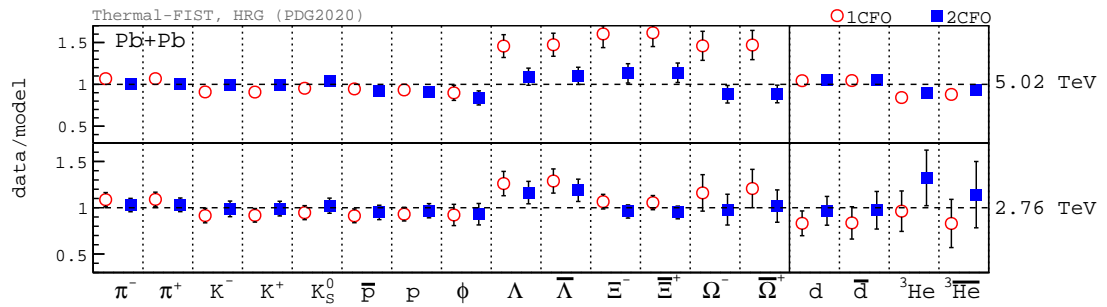


Figure 4: Ratios of experimental data to thermal model fit to  $\pi$ ,  $K$ ,  $K_s^0$ ,  $p$ ,  $\phi$ ,  $\Lambda$ ,  $\Xi$ ,  $\Omega$ ,  $d$ , and  ${}^3\text{He}$  in 0–10% centrality of Pb+Pb collisions at  $\sqrt{s_{NN}} = 2.76$  and 5.02 TeV following the same symbol convention as Fig. 3.

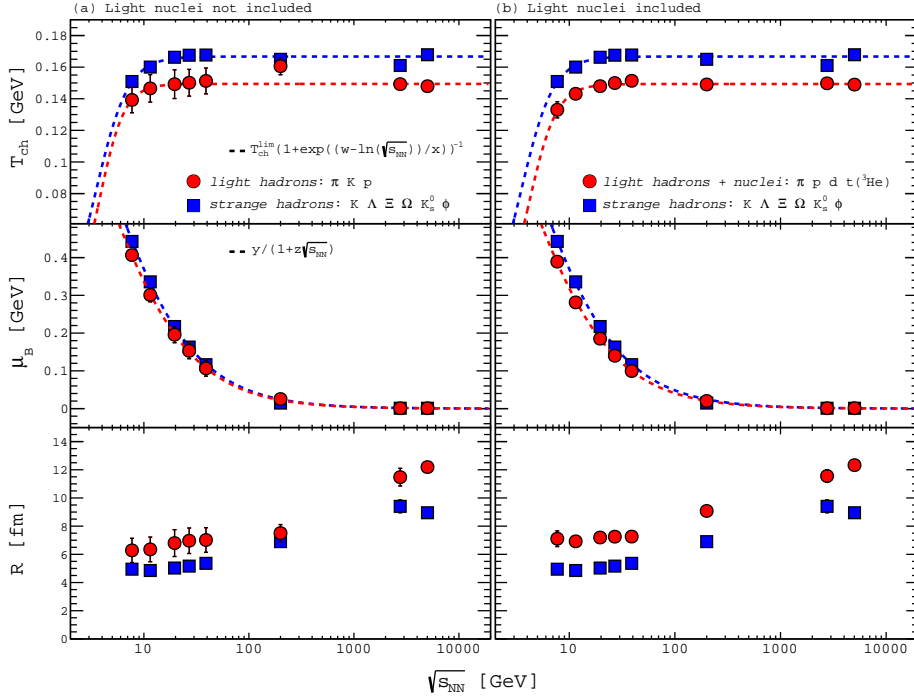


Figure 5: Fit parameters  $T_{ch}$ ,  $\mu_B$ , and  $R$  for 2CFO scenario extracted from thermal fits to identified hadrons (a) without and (b) with the inclusion of light nuclei.

Table 1: Fit parameters from parametrization of  $T_{ch}$  and  $\mu_B$  for different particle sets.

Parameters	1CFO		2CFO		
	<i>hadrons</i>	<i>hadrons+nuclei</i>	<i>light hadrons</i>	<i>light hadrons+nuclei</i>	<i>strange hadrons</i>
$T_{ch}^{lim}$ (MeV)	$162.87 \pm 0.67$	$153.14 \pm 0.28$	$149.40 \pm 1.50$	$149.33 \pm 0.40$	$166.71 \pm 0.88$
$w$	1.46	1.59	1.32	1.43	1.27
$x$	0.24	0.17	0.28	0.30	0.35
$y$ (GeV)	1.39	1.46	1.28	1.32	1.41
$z$ (GeV $^{-1}$ )	0.28	0.37	0.28	0.31	0.28

tios,  $d/p$ ,  $\bar{d}/\bar{p}$ ,  $t/p$ , and  $t/d$ . The results from the 1CFO and 2CFO calculations are compared to determine which scenario better describes the experimentally reported nuclei yield ratios.

### 3. Results

Figures 1 and 2 present the ratios of the experimentally measured  $dN/dy$  yields of various hadrons to the corresponding values obtained from thermal fits in both the 1CFO and 2CFO scenarios. Figure 1 shows results for Au+Au collisions at  $\sqrt{s_{NN}} = 7.7 - 200$  GeV, while Fig. 2 illustrates results for Pb+Pb collisions at  $\sqrt{s_{NN}} =$

2.76 and 5.02 TeV.

In Au+Au collisions, we observe that both the 1CFO and 2CFO scenarios are in a good agreement with the data for strange hadrons, but the 2CFO scenario achieves a better match with  $\pi$  and  $p$  yields. At LHC energies, the 2CFO scenario demonstrates a noticeable overall improvement in agreement with the experimental data across all particle species.

We also examine the impact of including light nuclei in the thermal fits, with the results shown in Figs. 3 and 4. Incorporating light nuclei into the fits significantly worsens the agreement of the 1CFO scenario, particularly for strange hadrons, whereas the 2CFO sce-

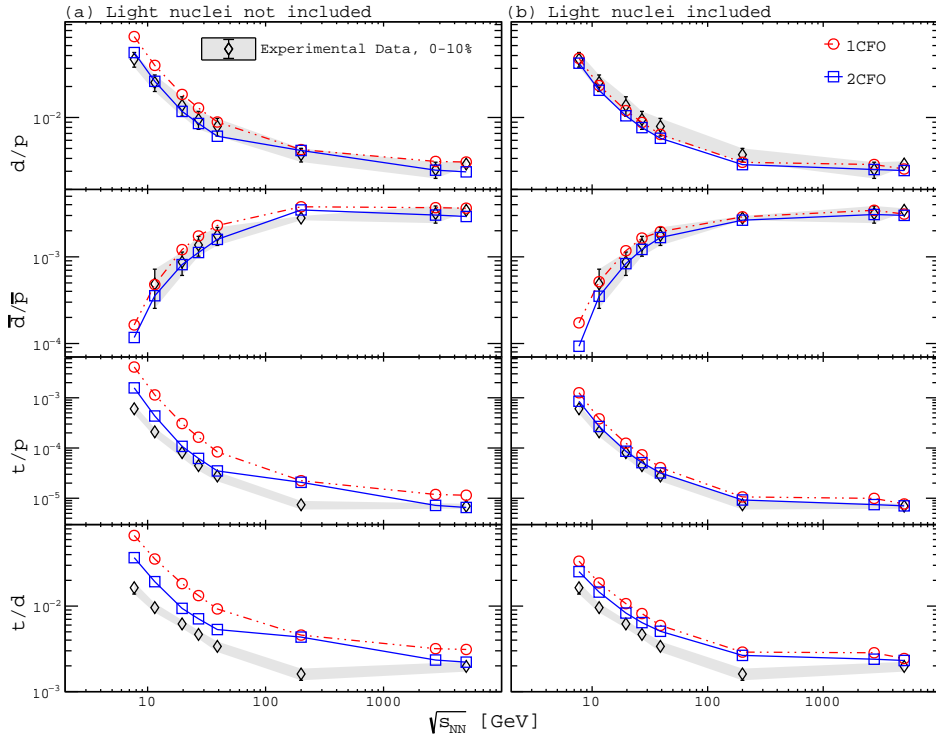


Figure 6: Comparison of light nuclei yield ratios with the thermal model. The ratios are calculated using the thermal parameters extracted from the chemical freeze-out parameters based on thermal fits to identified hadrons without the inclusion of light nuclei.

nario continues to provide a better match with the experimental data. For light nuclei at RHIC energies, we find that while the yield of  $d$  shows little improvement in the 2CFO scenario compared to 1CFO, the yields of  $t$  and  $\bar{d}$  is better described in the 2CFO scenario. At LHC energies, the 2CFO scenario demonstrates an overall improvement in agreement with the experimental yields of light nuclei compared to the 1CFO scenario.

The variations of  $T_{\text{ch}}$ ,  $\mu_B$ , and radius  $R$  with  $\sqrt{s_{\text{NN}}}$  extracted within 2CFO scenario with and without light nuclei included in the thermal fits are shown in Fig. 5. Detailed fit results for each energy and particle sets in both 1CFO and 2CFO scenarios have been listed in Table A1. We observe that  $T_{\text{ch}}$  of *light hadrons(+nuclei)* set is consistently lower than that of *strange hadrons* set by 10-20 MeV. This, along with the larger radius of the fireball for *light hadrons(+nuclei)* set, suggests that light hadrons and nuclei freeze out later in the evolution of the hadronic fireball compared to the strange hadrons. We also observe that  $\mu_B$  does not differ much between *light hadrons(+nuclei)* and *strange hadrons* sets in agreement with previous observations [15]. The energy dependence of  $T_{\text{ch}}$  and  $\mu_B$  can be parametrised

as [37],

$$T_{\text{ch}} = T_{\text{ch}}^{\text{lim}} \frac{1}{1 + \exp\left(\frac{w - \ln(\sqrt{s_{\text{NN}}})}{x}\right)}, \text{ and} \quad (2)$$

$$\mu_B = \frac{y}{1 + z\sqrt{s_{\text{NN}}}}, \quad (3)$$

where  $T_{\text{ch}}^{\text{lim}}$  is the limiting temperature. The fit values of these parameters have been summarized in Table 1.

We use thermal parameters obtained from the fits to *hadrons(+nuclei)* and *light hadrons(+nuclei)* sets to calculate light nuclei yield ratios,  $d/p$ ,  $\bar{d}/\bar{p}$ ,  $t/p$ , and  $t/d$  in the 1CFO and 2CFO scenarios, respectively. Figure 6 compares these calculations as a function of  $\sqrt{s_{\text{NN}}}$  in the 0–10% centrality class of Au+Au and Pb+Pb collisions. The figure is split into two panels: (a) light nuclei not included in the fit, and (b) light nuclei included. Both panels show results for the two different freeze-out scenarios, 1CFO and 2CFO, along with the STAR and ALICE data. We observe that,

- for the  $d/p$  ratio, the 1CFO scenario tends to overestimate the experimental results, particularly at lower  $\sqrt{s_{\text{NN}}}$ , and agrees with the data only when



light nuclei are included in the fit. In contrast, the 2CFO scenario consistently reproduces the experimental values within uncertainties.

- for the  $\bar{d}/\bar{p}$  ratio, both the 1CFO and 2CFO scenario describe the data within uncertainties and inclusion of light nuclei in the thermal fits only improves the agreement with the experimental data at both RHIC and LHC energies.
- for the  $t/p$  ratio, the 1CFO scenario consistently overestimates the experimental data across all studied  $\sqrt{s_{NN}}$ . In contrast, the 2CFO scenario provides a good agreement with the data for  $\sqrt{s_{NN}} > 19$  GeV, except for Au+Au collisions at  $\sqrt{s_{NN}} = 200$  GeV. Including light nuclei in the fit improves the agreement of the 2CFO scenario with the experimental results and also leads to a moderate improvement in the 1CFO scenario for  $\sqrt{s_{NN}} > 19$  GeV.
- for the  $t/d$  ratio, both scenarios overestimate the experimental data at RHIC energies, irrespective of whether light nuclei are included in the thermal fit. However, the 2CFO scenario both with and without light nuclei, and the 1CFO scenario with light nuclei included, show reasonable agreement with the observed data for Pb+Pb collisions at  $\sqrt{s_{NN}} = 5.02$  TeV.

Our findings suggest that the 2CFO scenario offers a more accurate description of identified hadrons with a particular emphasis on light nuclei production, showing better agreement with both light nuclei yields and their ratios. Notably, the inclusion of light nuclei in the thermal fits improves the agreement of both the 1CFO and 2CFO scenarios with the experimentally measured light nuclei yield ratios across various particle sets. Although an improvement to the calculated light-nuclei yield ratios is present within the 1CFO scenario, it is worth noting the individual yield calculations worsen for all hyperons.

#### 4. Summary

We studied particle production in Au+Au collisions at RHIC energies and Pb+Pb collisions at LHC energies using the HRG model framework, focusing on the flavor-dependent chemical freeze-out and its impact on light nuclei production. The analysis was conducted using the Thermal-FIST package under the Grand Canonical Ensemble (GCE) formalism, with quantum statistics applied to all particles.

Thermal parameters,  $T_{ch}$  and  $\mu_B$ , were determined in both the 1CFO and 2CFO scenarios by performing thermal fits to various particle sets. The effect of light nuclei on the chemical freeze-out was also studied by incorporating them into the thermal fits.

The extracted thermal parameters suggest a flavour hierarchy in the freeze-out process, indicating that strange hadrons decouple earlier in the evolution of the hadronic fireball compared to light hadrons across all studied collision energies.

To further understand the impact of the 2CFO scenario on light nuclei production, we examined the yield ratios of light nuclei,  $d/p$ ,  $\bar{d}/\bar{p}$ ,  $t/p$ , and  $t/d$ , using thermal parameters obtained from fits in both 1CFO and 2CFO scenarios. The 2CFO scenario consistently provides a better description of these ratios than the 1CFO scenario, although challenges remain, particularly in addressing the overestimation of the  $t/d$  ratio at RHIC energies.

This study supports the flavour-dependent freeze-out at RHIC and LHC energies, suggesting that strange and light hadrons (including light nuclei) may freeze out at different temperatures. This letter emphasizes the importance of considering a flavour-dependent chemical freeze-out when including light nuclei in the thermal model framework as well as extending future analyses to hypernuclei and beyond.

#### Acknowledgments

CJ acknowledges the financial support from DAE-DST, Government of India bearing Project No. SR/MF/PS-02/2021-IISERT (E-37130). FAF and HC acknowledge the DOE grant DE-SC004168 for supporting this work. Additionally, FAF would like to thank the National Science Foundation Grant No. 2138010.

#### References

- [1] J. Adams *et al.* (STAR Collaboration), *Nucl. Phys. A* **757**, 102 (2005).
- [2] Y. Aoki, G. Endrodi, Z. Fodor, S. D. Katz, and K. K. Szabo, *Nature* **443**, 675 (2006).
- [3] S. Ejiri, *Phys. Rev. D* **78**, 074507 (2008).
- [4] S. Acharya *et al.* (ALICE Collaboration), *Eur. Phys. J. C* **84**, 813 (2024).
- [5] S. Chatterjee, S. Das, L. Kumar, D. Mishra, B. Mohanty, R. Sahoo, and N. Sharma, *Adv. High Energy Phys.* **2015**, 349013 (2015).
- [6] J. Cleymans and K. Redlich, *Phys. Rev. Lett.* **81**, 5284 (1998).
- [7] F. Becattini, in *International School on Quark-Gluon Plasma and Heavy Ion Collisions: past, present, future* (2009) [arXiv:0901.3643 \[hep-ph\]](https://arxiv.org/abs/0901.3643).
- [8] A. Andronic, P. Braun-Munzinger, K. Redlich, and J. Stachel, *Nature* **561**, 321 (2018).

- [9] S. Chatterjee, R. M. Godbole, and S. Gupta, *Phys. Lett. B* **727**, 554 (2013).
- [10] K. A. Bugaev, D. R. Oliinychenko, J. Cleymans, A. I. Ivanytskyi, I. N. Mishustin, E. G. Nikonov, and V. V. Sagun, *EPL* **104**, 22002 (2013).
- [11] S. Chatterjee and B. Mohanty, *Phys. Rev. C* **90**, 034908 (2014).
- [12] C. Ratti, R. Bellwied, M. Cristoforetti, and M. Barbaro, *Phys. Rev. D* **85**, 014004 (2012).
- [13] R. Bellwied, S. Borsanyi, Z. Fodor, S. D. Katz, and C. Ratti, *Phys. Rev. Lett.* **111**, 202302 (2013).
- [14] F. A. Flor, G. Olinger, and R. Bellwied, *Phys. Lett. B* **814**, 136098 (2021).
- [15] F. A. Flor, G. Olinger, and R. Bellwied, *Phys. Lett. B* **834**, 137473 (2022).
- [16] A. Andronic, P. Braun-Munzinger, J. Stachel, and H. Stoecker, *Phys. Lett. B* **697**, 203 (2011).
- [17] N. Yu, Z. Zhang, H. Xu, and M. Song, (2024), [arXiv:2403.16548 \[nucl-th\]](https://arxiv.org/abs/2403.16548).
- [18] D. Oliinychenko, *Nucl. Phys. A* **1005**, 121754 (2021).
- [19] P. J. Siemens and J. I. Kapusta, *Phys. Rev. Lett.* **43**, 1486 (1979).
- [20] D. Hahn and H. Stoecker, *Nucl. Phys. A* **476**, 718 (1988).
- [21] J. Adam *et al.* (STAR Collaboration), *Phys. Rev. C* **99**, 064905 (2019).
- [22] M. Abdulhamid *et al.* (STAR Collaboration), *Phys. Rev. Lett.* **130**, 202301 (2023).
- [23] V. Vovchenko and H. Stoecker, *Comput. Phys. Commun.* **244**, 295 (2019).
- [24] P. A. Zyla *et al.* (Particle Data Group), *PTEP* **2020**, 083C01 (2020).
- [25] J. Adams *et al.* (STAR Collaboration), *Phys. Lett. B* **612**, 181 (2005).
- [26] J. Adam *et al.* (STAR Collaboration), *Phys. Rev. C* **102**, 034909 (2020).
- [27] L. Adamczyk *et al.* (STAR Collaboration), *Phys. Rev. C* **96**, 044904 (2017).
- [28] F. Bellini (ALICE Collaboration), *Nucl. Phys. A* **982**, 427 (2019).
- [29] S. Acharya *et al.* (ALICE Collaboration), *Phys. Rev. C* **107**, 064904 (2023).
- [30] S. Acharya *et al.* (ALICE Collaboration), *Phys. Rev. C* **101**, 044907 (2020).
- [31] B. B. Abelev *et al.* (ALICE Collaboration), *Phys. Rev. C* **91**, 024609 (2015).
- [32] S. Acharya *et al.* (ALICE Collaboration), *Phys. Rev. Lett.* **133**, 092301 (2024).
- [33] B. I. Abelev *et al.* (STAR Collaboration), *Phys. Rev. C* **79**, 034909 (2009).
- [34] G. Agakishiev *et al.* (STAR Collaboration), *Phys. Rev. Lett.* **108**, 072301 (2012).
- [35] V. Vovchenko, M. I. Gorenstein, and H. Stoecker, *Phys. Rev. C* **98**, 034906 (2018).
- [36] D. Magestro, *J. Phys. G* **28**, 1745 (2002).
- [37] A. Andronic, P. Braun-Munzinger, and J. Stachel, *Phys. Lett. B* **673**, 142 (2009), [Erratum: *Phys. Lett. B* 678, 516 (2009)].



Table A1: Fit parameters for different freeze-out scenarios at various collision energies.

$\sqrt{s_{NN}}$ (GeV)	$T$ (MeV)	$\mu_B$ (MeV)	Radius (fm)	$\chi^2/\text{ndf}$
<i>1CFO hadrons: <math>\pi, K, K_s^0, p, \phi, \Lambda, \Xi, \text{ and } \Omega</math></i>				
7.7	$149.96 \pm 1.75$	$436.28 \pm 11.98$	$5.06 \pm 0.18$	19.9/9
11.5	$158.73 \pm 1.60$	$328.67 \pm 10.39$	$5.00 \pm 0.15$	34.6/11
19.6	$165.19 \pm 1.34$	$213.92 \pm 5.93$	$5.14 \pm 0.13$	25.4/11
27	$166.66 \pm 1.30$	$161.16 \pm 5.82$	$5.26 \pm 0.12$	31.8/11
39	$165.82 \pm 1.84$	$112.06 \pm 8.30$	$5.56 \pm 0.18$	16.0/11
200	$162.95 \pm 1.85$	$20.44 \pm 10.25$	$7.21 \pm 0.23$	27.8/10
2760	$156.67 \pm 1.99$	1.0	$10.20 \pm 0.38$	17.8/12
5020	$156.13 \pm 1.63$	1.0	$10.71 \pm 0.31$	70.1/12
<i>1CFO hadrons+nuclei: <math>\pi, K, K_s^0, p, \phi, \Lambda, \Xi, \Omega, d, \text{ and } t \text{ or } ^3\text{He}</math></i>				
7.7	$143.14 \pm 1.05$	$381.02 \pm 3.50$	$5.85 \pm 0.12$	55.5/11
11.5	$151.43 \pm 0.90$	$275.70 \pm 3.06$	$5.75 \pm 0.10$	81.7/14
19.6	$156.52 \pm 0.75$	$177.81 \pm 2.41$	$6.00 \pm 0.09$	117.3/14
27	$158.04 \pm 0.70$	$132.48 \pm 2.32$	$6.07 \pm 0.08$	123.7/14
39	$156.03 \pm 0.87$	$96.93 \pm 2.78$	$6.54 \pm 0.12$	68.9/14
200	$151.56 \pm 0.78$	$17.80 \pm 2.74$	$8.66 \pm 0.15$	91.2/13
2760	$153.93 \pm 1.32$	1.0	$10.69 \pm 0.29$	22.9/16
5020	$150.17 \pm 0.42$	1.0	$11.89 \pm 0.13$	101.1/16
<i>2CFO light hadrons: <math>\pi, K, \text{ and } p</math></i>				
7.7	$139.24 \pm 8.11$	$406.56 \pm 15.06$	$6.28 \pm 0.86$	1.7/3
11.5	$146.56 \pm 8.68$	$301.07 \pm 18.35$	$6.35 \pm 0.88$	2.9/3
19.6	$149.22 \pm 9.08$	$195.82 \pm 21.28$	$6.80 \pm 0.95$	4.5/3
27	$150.13 \pm 8.46$	$153.00 \pm 20.88$	$6.97 \pm 0.90$	3.2/3
39	$151.28 \pm 8.17$	$106.58 \pm 20.71$	$7.02 \pm 0.87$	3.1/3
200	$160.60 \pm 5.40$	$25.31 \pm 14.26$	$7.51 \pm 0.61$	3.9/3
2760	$149.25 \pm 3.15$	1.0	$11.48 \pm 0.63$	4.5/4
5020	$147.93 \pm 1.89$	1.0	$12.19 \pm 0.40$	11.4/4
<i>2CFO light hadrons+nuclei: <math>\pi, p, d, \text{ and } t \text{ or } ^3\text{He}</math></i>				
7.7	$133.03 \pm 5.11$	$389.27 \pm 12.59$	$7.11 \pm 0.56$	2.0/3
11.5	$143.14 \pm 3.34$	$281.28 \pm 9.74$	$6.92 \pm 0.37$	5.3/4
19.6	$147.97 \pm 1.73$	$185.21 \pm 5.45$	$7.20 \pm 0.26$	3.5/4
27	$149.94 \pm 1.36$	$139.88 \pm 4.12$	$7.25 \pm 0.23$	5.3/4
39	$151.36 \pm 1.24$	$99.49 \pm 3.57$	$7.26 \pm 0.23$	7.3/4
200	$149.03 \pm 0.95$	$20.26 \pm 3.23$	$9.08 \pm 0.21$	15.2/4
2760	$149.76 \pm 1.88$	1.0	$11.56 \pm 0.45$	2.2/6
5020	$148.96 \pm 0.52$	1.0	$12.33 \pm 0.19$	18.2/6
<i>2CFO strange hadrons: <math>K, K_s^0, \phi, \Lambda, \Xi, \text{ and } \Omega</math></i>				
7.7	$150.91 \pm 1.82$	$442.75 \pm 13.50$	$4.95 \pm 0.18$	11.9/5
11.5	$160.03 \pm 1.67$	$335.69 \pm 11.44$	$4.85 \pm 0.16$	20.1/7
19.6	$166.24 \pm 1.39$	$217.44 \pm 6.25$	$5.03 \pm 0.13$	10.2/7
27	$167.53 \pm 1.34$	$163.00 \pm 6.10$	$5.16 \pm 0.12$	18.4/7
39	$167.67 \pm 1.99$	$116.38 \pm 9.42$	$5.36 \pm 0.19$	6.6/7
200	$164.95 \pm 2.15$	$14.59 \pm 14.79$	$6.90 \pm 0.27$	22.69/6
2760	$161.05 \pm 2.51$	1.0	$9.40 \pm 0.45$	5.6/8
5020	$167.86 \pm 2.23$	1.0	$8.95 \pm 0.32$	11.2/8